

Emergence of momentum-space topological half vortices in an anisotropic cavity

Xingqi Zhao,^{1,§} Jiajun Wang^{1,*,§} Xinhao Wang,¹ Lei Shi^{1,2,3,4,†} and Jian Zi^{1,2,3,4,‡}

¹State Key Laboratory of Surface Physics, Key Laboratory of Micro- and Nano-Photonic Structures (Ministry of Education) and Department of Physics, Fudan University, 200433 Shanghai, China

²Institute for Nanoelectronic Devices and Quantum Computing, Fudan University, 200438 Shanghai, China

³Collaborative Innovation Center of Advanced Microstructures, Nanjing University, Nanjing, 210093 Jiangsu, China

⁴Shanghai Research Center for Quantum Sciences, 201315 Shanghai, China



(Received 19 January 2023; revised 27 September 2023; accepted 8 November 2023; published 29 November 2023)

Topological half vortices in momentum space have recently attracted great interest in photonic research. Characterized by winding polarization distributions, topological half vortices carry half-integer topological charges, underlying many exotic optical phenomena. To date, in systems with continuous translational symmetry, the study of momentum-space topological vortices is based mostly on the band degeneracies. Here we theoretically propose that by optical cavities that contain uniaxial materials, two types of momentum-space topological half vortex can emerge. With both a Hamiltonian model and eigenmode simulations, we reveal that paired degenerate and nondegenerate half vortices can be spawned from zero topological charge with different energy detuning of bands. The winding configurations of topological half vortices are closely associated with the distinctive characteristics of Berry curvature. Our work broadens methods to generate and manipulate topological half vortices in momentum space, and also offers a perspective of polarization vortices in the investigation of cavity photons in anisotropic media.

DOI: 10.1103/PhysRevApplied.20.054059

I. INTRODUCTION

Topological vortices, which are universal in real space, have been widely discussed in various fields, such as superfluids [1], superconductors [2], and exciton–polariton condensates [3]. In recent photonic research, topological vortices were also discovered to exist in momentum space, known as momentum-space polarization vortices [4–7]. For these polarization vortices, major axes of states of polarization (SOPs) will wind around specific vortex centers in momentum space, causing nonzero winding numbers (topological charges). Topological charges can be integers; for example, the SOPs will wind around bound states in the continuum, forming polarization vortices with integer topological charges [8–18]. Besides, topological charges can also be half-integers [19–27]. Polarization vortices with half-integer charges (topological half vortices) can be divided into two cases with different vortex centers. For the nondegenerate case (nondegenerate half vortices), vortex centers are circularly polarized states (C points), which are radiative states with circular SOPs. Because of chiral responses of C points, nondegenerate

half vortices have provided significant applications in chiral emission, light-matter interactions, etc [28–33]. For the degenerate case (degenerate half vortices), vortex centers are degenerate points, whose SOPs are undefined owing to the arbitrary superposition of modes at band degeneracies [19,21,34]. Exhibiting abundant topological features, degenerate half vortices are closely associated with a non-trivial Berry phase, and have also resulted in exotic discoveries in non-Hermitian physics, such as exceptional points [19,34].

The light field with various topological half vortices has been studied previously. For example, various polarization configurations, such as C points, have been explored in propagation waves in media uniformly distributed in three dimensions [35]. When light beams propagate through a bulky crystal, the topological-half-vortex features can also be passively obtained by propagation-induced modulation [36–38]. Recently, with the rapid development of microphotonics and nanophotonics, the emergence of compact photonic structures brings new degrees of freedom in light-field modulation. These compact photonic structures, such as photonic crystal slabs [39], support optical eigenmodes that can interact with light in free space. On the one hand, when satisfying the condition of momentum matching, the optical modes can radiate into free space, and their SOPs can form an eigenpolarization field in momentum space, including various topological half vortices [25]. On

*jiajunwang@fudan.edu.cn

†lshi@fudan.edu.cn

‡jzi@fudan.edu.cn

§These authors contributed equally to this work.

the other hand, the optical modes can also be excited by light from free space, and the existence of topological half vortices will give rise to a wide range of effects in the resonant process [18].

In microphotonics and nanophotonics, the topological half vortices in momentum space have rich physical significance to be further explored. To fully investigate and utilize the properties of topological half vortices, the generation and modulation of topological half vortices are of vital importance. Breaking symmetries and varying structural parameters are commonly applied methods, with which various evolutions of topological half vortices have been explored [20–24,26,27,40]. On the one hand, topological half vortices can be spawned from integer-charge vortices. For instance, a pair of nondegenerate half vortices can be spawned from an integer-charge vortex centered at a bound state in the continuum by the breaking of the in-plane inversion symmetry or up-down mirror symmetry [20,22]; a pair of degenerate half vortices can be generated from an integer-charge degenerate vortex by variation of the in-plane symmetry from C_{4v} to C_{2v} [19,21]. On the other hand, topological half vortices can also be generated from zero charge; for example, paired nondegenerate half vortices with opposite-signed charges can emerge by the shifting of the misalignment of a double-layer-grating structure [26]. In these previous studies, topological half vortices were mostly realized and discussed in periodic structures with discrete translational symmetry, such as photonic crystal slabs. Besides periodic structures, photonic systems with continuous translational symmetry also have well-defined momentum space, but the topological half vortices in these systems have not been fully investigated.

So far, the study of momentum-space topological vortices in continuous photonic systems has been based mostly on degenerate points [41–45]. In planar optical microcavities, degenerate half vortices have been realized, associated with various effects such as conical diffraction and non-Abelian gauge fields [41,44]. Recently, it was found that Rashba-Dresselhaus (RD) coupling will lead to the chirality of modes [46], which has attracted much research interest and has been used to realize various applications [47–55]. However, nondegenerate half vortices in these systems have not been revealed to date. To promote further research and practical applications, it is still worth exploring new mechanisms to generate and modulate topological half vortices.

In this study, we propose a general approach to generating and modulating two types of topological half vortex in optical cavities containing uniaxial media. On the basis of systems with continuous translational symmetry, we focus on cavity modes of two bands with different parities. Accompanied by different energy detuning of bands, we show that paired degenerate and nondegenerate half vortices can be spawned from zero topological charge.

The topological half vortices are paired and carry opposite topological charges, maintaining the conservation of total topological charges. The winding topology of SOPs and RD coupling will lead to distinctive characteristics in Berry curvature. Two types of vortex center, half-charge degenerate points and C points, can be directly characterized by linearly polarized and circularly polarized reflectance spectra.

II. RESULTS AND DISCUSSION

Our platform is constructed by our embedding a uniaxial layer in a pair of distributed Bragg reflectors (DBRs), as is shown in the middle panel in Fig. 1(a). Owing to constraints along the z direction and continuous translational symmetry in the x - y plane, this structure supports cavity modes with well-defined in-plane wave vector $\mathbf{k}_{\parallel} = (k_x, k_y)$. The optical axis of the uniaxial layer is set in the x - z plane with a tilt angle θ relative to the x axis. Here we are focusing on a transverse electric (TE) band and a transverse magnetic (TM) band, which are energetically close and of different parities. In the parabolic approximation and with the radiation loss ignored, this two-band system can be described by a 2×2 effective Hamiltonian in the circular-polarization basis [45–47]:

$$H = E_0 + \frac{\hbar^2 k_x^2}{2m_x} + \frac{\hbar^2 k_y^2}{2m_y} + \begin{pmatrix} -2\alpha k_y & \beta_0 - \beta_1 k_{\parallel}^2 + \beta_2 k_{\parallel}^2 e^{-2i\varphi} \\ \beta_0 - \beta_1 k_{\parallel}^2 + \beta_2 k_{\parallel}^2 e^{2i\varphi} & 2\alpha k_y \end{pmatrix}, \quad (1)$$

where E_0 is the mean mode energy, m_x and m_y are the effective masses of cavity photons, α represents the RD coupling between cavity modes with different parities, β_0 represents the detuning of the modes' energy at $\mathbf{k}_{\parallel} = 0$ (it can be dynamically controlled by variation of the tilt angle θ), β_1 and β_2 contribute to the TE-TM splitting and TE-TM spin-orbital coupling, and φ is the propagation angle following $k_x = k_{\parallel} \cos \varphi$ and $k_y = k_{\parallel} \sin \varphi$. By obtaining the eigensolutions of the Hamiltonian model, one can determine the SOPs of the modes. In our discussions, the wave vectors considered are relatively small, and hence the x and y components are applied to define the SOPs.

With the variation of β_0 , two types of topological half vortex will emerge from zero topological charge. When $\beta_0 < 0$, the two bands are separated, as shown in the left panel in Fig. 1(a). In this case, there is no polarization singularity on both bands and the topological charge of this region is zero [left panel in Fig. 1(b)]. When $\beta_0 > 0$, polarization singularities emerge along both the k_x direction and the k_y direction. On the one hand, the bands intersect at $(k_x, k_y) = (\pm\sqrt{\beta_0}/(\beta_1 - \beta_2), 0)$, forming two degenerate points. On the other hand, the modes will become fully

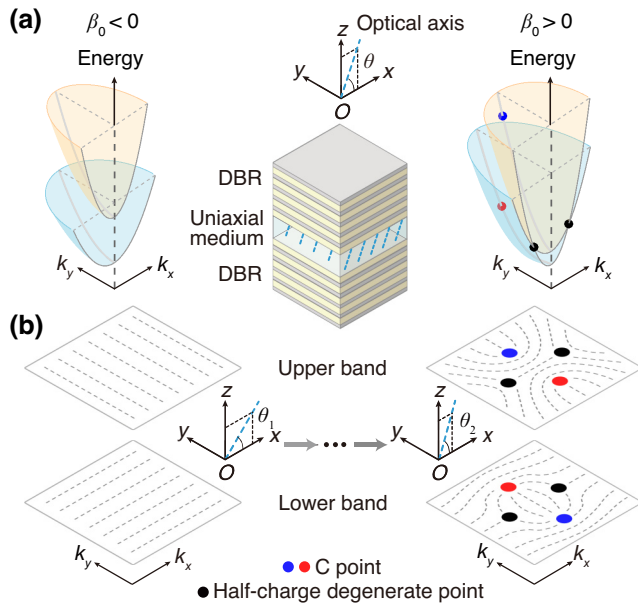


FIG. 1. (a) Schematic view of the structure (middle panel) and energy dispersions of modes at a negative detuning and a positive detuning (left and right panels). (b) Polarization distributions of upper and lower bands in (a). Dashed lines represent major axes of SOPs, red and blue dots represent LCP and RCP C points, respectively, and black dots represent half-charge degenerate points.

circular at $(k_x, k_y) = (0, \pm\sqrt{\beta_0}/(\beta_1 + \beta_2))$, corresponding to C points. In the vicinity of these polarization singularities, the major axis of SOPs exhibits winding topology, forming both degenerate and nondegenerate half vortices, as shown in the right panel in Fig. 1(b). Around a degenerate half vortex, the major axis of SOPs winds by $-\pi$, corresponding to a $-1/2$ topological charge, while around a nondegenerate half vortex, the major axis of SOPs winds by $+\pi$, corresponding to a $+1/2$ topological charge. In this region, the total topological charges of both the upper band and the lower band are always zero, maintaining the conservation law of topological charges.

To give a specific example of the generation and evolution of topological half vortices, we set a liquid crystal as the uniaxial layer. A liquid crystal is a commonly used uniaxial anisotropic medium, whose optical axis can be tuned by application of an external voltage [46,56–59]. In our discussions, the liquid crystal is of positive birefringence ($n_o = 1.59, n_e = 2.18$) [57,59], and its thickness is $1.6 \mu\text{m}$. The DBRs are designed with use of SiO_2 and TiO_2 layers to make the bands concerned be located in the band gap (details are provided in Supplemental Material [60]).

To exhibit the energy evolution caused by rotation of the optical axis, we calculated bands at different tilt angles. First, we focus our discussion on a TE band with mode number N and a TM band with mode number $N + 1$, denoted by $(N, N + 1)$. In this regime, we plot the band

dispersions and polarization distributions of a negative detuning ($\beta_0 = -17.2 \text{ meV}$) and a positive detuning ($\beta_0 = 1.79 \text{ meV}$) in the left and middle columns in Fig. 2. The energy dispersions of bands along the k_x direction [Fig. 2(a)] are separated when $\beta_0 < 0$, while they intersect with each other when $\beta_0 > 0$. In contrast, along the k_y direction [Fig. 2(b)], the two bands will not intersect with each other for both positive and negative β_0 . Figures 2(c) and 2(d) show corresponding polarization distributions of the upper band and the lower band, respectively. When $\beta_0 < 0$, in both the upper band and the lower band, the major axis of the SOPs points in nearly the same direction, meaning that no topological vortex exists. When β_0 becomes positive, paired degenerate and nondegenerate half vortices emerge in both the upper band and the lower band, in correspondence with our discussion from the Hamiltonian model.

By varying the optical axis, we can also realize the emergence of topological half vortices in the $(N, N + 3)$ regime, as shown in the right column in Fig. 2. The band dispersions and polarization distributions in this case are similar to those in the $(N, N + 1)$ case. However, in this regime, the energy splitting of modes along the k_y direction is much smaller than that in the $(N, N + 1)$ regime, indicating that the strength of RD coupling is weaker in this case. From the band dispersions, we extracted the strength of RD coupling, which is $3.53 \text{ meV} \cdot \mu\text{m}$ in the $(N, N + 1)$ case and $1.08 \text{ meV} \cdot \mu\text{m}$ in the $(N, N + 3)$ case. The different RD couplings will lead to different characteristics of the distributions of SOPs: In the $(N, N + 1)$ case, the SOPs are very close to circular in a large area around the C point. In contrast, in the $(N, N + 3)$ case, only a small area near the C point has a high degree of circular polarization.

The winding configuration of SOPs are closely connected with some intrinsic topological natures of the system, e.g., nonzero Berry curvature. The Berry curvature can be calculated by [47,61,62]

$$\Omega = \frac{1}{2} \sin \Theta (\partial_{k_x} \Theta \partial_{k_y} \Phi - \partial_{k_x} \Phi \partial_{k_y} \Theta), \quad (2)$$

where Θ and Φ are the polar and azimuthal angles of the Poincaré sphere, defined by $\Theta = \arccos(S_3/S_0)$ and $\Phi = \arctan(S_2/S_1)$ (where S_0, S_1, S_2 , and S_3 are Stokes parameters). From this perspective, the distribution of Berry curvature is closely related to the changing rate of SOPs in momentum space. We show the distribution of Berry curvature of the upper band from the Hamiltonian model in Fig. 3(a) and from numerical simulation in Fig. 3(b). The Berry-curvature distributions are calculated by using the SOPs of nondegenerate optical modes; the cases of degenerate points with ill-defined SOPs are outside the scope of this work. In the calculation of Berry curvature by the Hamiltonian model, the non-Hermiticity due to radiation

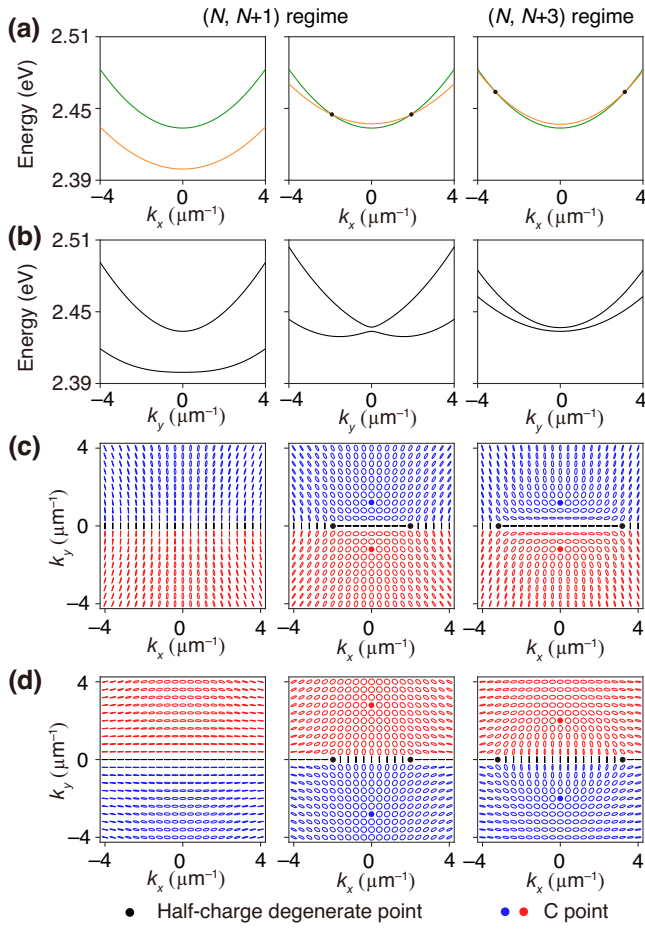


FIG. 2. Evolutions of dispersions and polarization distributions. The left column and the middle column correspond to $\beta_0 < 0$ and $\beta_0 > 0$, respectively, in the $(N, N + 1)$ regime. The right column corresponds to $\beta_0 > 0$ in the $(N, N + 3)$ regime. (a) Dispersions along the k_x direction. Green (orange) lines correspond to TE (TM) bands. (b) Dispersions along the k_y direction. (c),(d) Polarization distributions of (c) the upper band and (d) the lower band. Red and blue dots represent LCP and RCP C points, respectively, and black dots represent half-charge degenerate points.

loss should also be taken into consideration (details are provided in Supplementary Material [60]).

In the $(N, N + 1)$ regime, when the two bands are widely separated and no topological half vortex exists at $\beta_0 < 0$ (left column in Fig. 3), the Berry curvature in the whole region is close to zero. In contrast, when the topological half vortices emerge at $\beta_0 > 0$ (middle column in Fig. 3), the distribution of Berry curvature around the topological half vortices appears with nonzero value and obviously varies. In this case, for the nondegenerate half vortices, the Berry curvature is relatively small at vortex centers (C points). In contrast, in the $(N, N + 3)$ regime, the Berry curvature at $\beta_0 > 0$ is shown in the right column

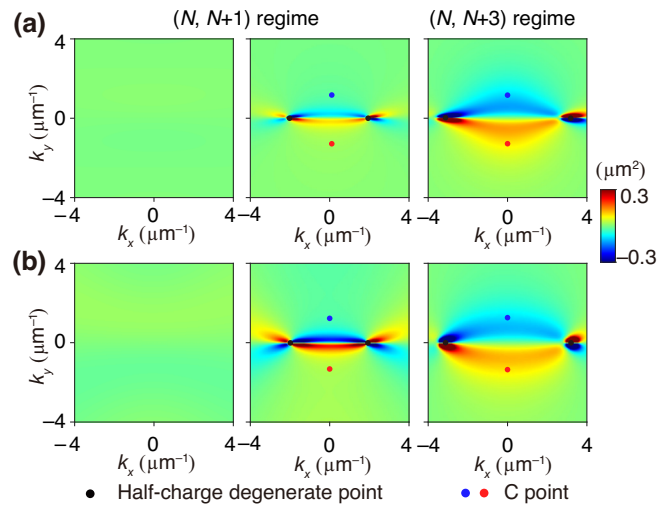


FIG. 3. Distributions of Berry curvature by (a) the Hamiltonian model and (b) numerical simulation. The left column and the middle column correspond to $\beta_0 < 0$ and $\beta_0 > 0$, respectively, in the $(N, N + 1)$ regime. The right column corresponds to $\beta_0 > 0$ in the $(N, N + 3)$ regime. Red and blue dots represent LCP and RCP C points, respectively, and black dots represent half-charge degenerate points.

in Fig. 3. In this case, nonzero Berry curvature significantly accumulates around the C points. The reason is that, in the $(N, N + 1)$ regime, the SOPs are very close to circular (e.g., $\Theta \approx 0$) in a wide range around the C points owing to a strong RD coupling. Thus, the Berry curvature around C points is relatively small in this case, while in the $(N, N + 3)$ regime, both the major axis and the ellipticity of the SOPs undergo drastic changes around the C points due to a relatively weak RD coupling, which will lead to the accumulation of Berry curvature around C points. In addition, when the RD coupling α becomes weaker, the Berry curvature will be more concentrated at C points (see Sec. 8 of Supplemental Material [60]).

The cavity modes in our discussion are above the light cone, and thus they can be excited by light incident on the structures, leading to obvious changes in reflection and transmission spectra. The resonance-induced spectra can manifest characteristics of both energy dispersions and SOPs of cavity modes. For the two types of topological half vortex discussed, there are different polarization-related responses for the far-field incidence, which can be used to characterize the generation and evolution of topological half vortices. Later, by applying Berreman's transfer-matrix method [63] (details are provided in Supplemental Material [60]), we calculated reflectance spectra along the k_x and k_y directions in the $(N, N + 3)$ regime, and found that they exhibit far-field polarization responses resulting from topological half vortices.

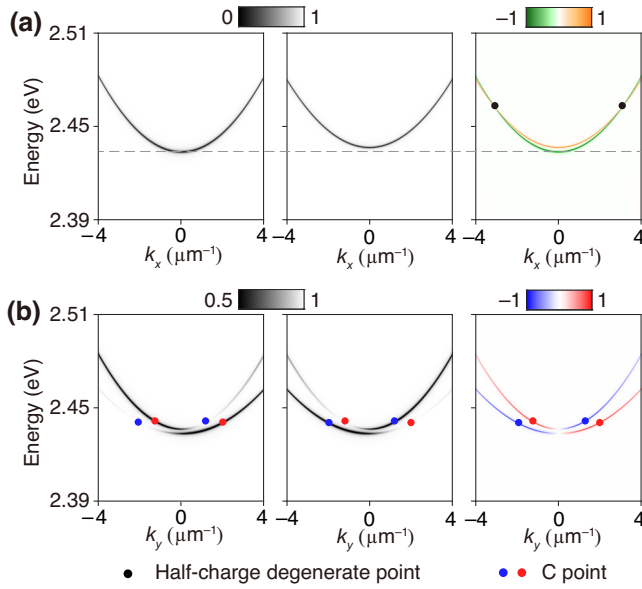


FIG. 4. (a) Reflectance spectra along the k_x direction under s -polarized and p -polarized incidence in the $(N, N + 3)$ case (left and middle panels) and calculated DLP of the reflection (right panel). (b) Reflectance spectra along the k_y direction under LCP and RCP incidence in the $(N, N + 3)$ case (left and middle panels) and calculated DCP of the reflection (right panel). Red and blue dots represent LCP and RCP C points and black dots represent half-charge degenerate points.

Figure 4(a) shows linearly polarized reflectance spectra along the k_x direction. The left and middle panels refer to reflectance spectra under s -polarized and p -polarized incidence, respectively. The TE (TM) modes cannot be excited by the p -polarized (s -polarized) incidence; therefore, the reflectance spectra under s -polarized (p -polarized) incidence correspond to responses of the TE (TM) band. In the right panel in Fig. 4(a), we also plot the degree of linear polarization (DLP), which is defined as $(R_s - R_p)/(R_s + R_p)$, where R_s (R_p) is the reflectance under s -polarized (p -polarized) incidence. For both the upper band and the lower band, there is a switch of signs of the DLP in the vicinity of band intersections, as shown in the right panel in Fig. 4(c). The sign changes of the DLP are in accordance with the polarization distributions shown in Figs. 2(c) and 2(d), where a transition of SOPs appears around a degenerate half vortex.

In Fig. 4(b), circularly polarized reflectance spectra along the k_y direction are shown that characterize optical responses related to nondegenerate half vortices. The left and middle panels refer to reflectance spectra under left-handed-circularly-polarized (LCP) and right-handed-circularly-polarized (RCP) incidence, respectively. There are diminished regions in the reflectance spectra, indicating the existence of C points. As centers of nondegenerate half vortices, C points cannot be excited by incidence with opposite circular polarization. These diminished regions in

the reflectance spectra for LCP and RCP incidence correspond to the RCP and LCP C points, which are marked by blue and red dots. Since the SOPs are close to circular only in a small area around the C points, the diminished regions are relatively narrow. Moreover, in the right panel of Fig. 4(b), we also show the degree of circular polarization (DCP), which is defined as $(R_r - R_l)/(R_r + R_l)$, where R_l (R_r) is the reflectance under LCP (RCP) incidence. Accompanied by the emergence of nondegenerate half vortices, the maximum DCP and the minimum DCP in the reflectance spectra approach ± 1 around the C points. It should be noted that, at $k_{\parallel} = 0$, the DCP is always zero due to the mirror symmetry. These results agree well with the polarization distribution in Figs. 2(c) and 2(d).

III. CONCLUSION

In conclusion, we have proposed an anisotropy-based mechanism to generate momentum-space topological half vortices. By just varying the optical axis of the uniaxial layer, we can realize the generation of two types of topological half vortex from zero topological charge. The emergence of topological half vortices will bring rich properties of Berry curvature and far-field polarization responses. Our results extend the investigation on topological half vortices in systems with continuous translational symmetry, and also demonstrate that optical cavities with anisotropic media can serve as good platforms for momentum-space polarization modulation.

ACKNOWLEDGMENTS

We thank Chang Shu for helpful discussions. The work was supported by the National Natural Science Foundation of China (Grants No. 12234007 and No. 12221004), the National Key R&D Program of China (Grants No. 2022YFA1404800 and No. 2021YFA1400603), the Major Program of the National Natural Science Foundation of China (Grant No. 91963212), and the Science and Technology Commission of Shanghai Municipality (Grants No. 22142200400, No. 21DZ1101500, and No. 2019SHZDZX01). J.W. was further supported by the Postdoctoral Innovative Talent Support Program of the China Postdoctoral Science Foundation (Grant No. BX20230079).

-
- [1] M. Salomaa and G. Volovik, Quantized vortices in superfluid ^3He , *Rev. Mod. Phys.* **59**, 533 (1987).
 - [2] G. Blatter, M. V. Feigel'man, V. B. Geshkenbein, A. I. Larkin, and V. M. Vinokur, Vortices in high-temperature superconductors, *Rev. Mod. Phys.* **66**, 1125 (1994).
 - [3] G. F. Q. Rosen, P. I. Tamborenea, and T. Kuhn, Interplay between optical vortices and condensed matter, *Rev. Mod. Phys.* **94**, 035003 (2022).

- [4] B. Zhen, C. W. Hsu, L. Lu, A. D. Stone, and M. Soljačić, Topological nature of optical bound states in the continuum, *Phys. Rev. Lett.* **113**, 257401 (2014).
- [5] C. W. Hsu, B. Zhen, A. D. Stone, J. D. Joannopoulos, and M. Soljačić, Bound states in the continuum, *Nat. Rev. Mater.* **1**, 16048 (2016).
- [6] Y. Zhang, A. Chen, W. Liu, C. W. Hsu, B. Wang, F. Guan, X. Liu, L. Shi, L. Lu, and J. Zi, Observation of polarization vortices in momentum space, *Phys. Rev. Lett.* **120**, 186103 (2018).
- [7] H. M. Doeleman, F. Monticone, W. den Hollander, A. Alù, and A. F. Koenderink, Experimental observation of a polarization vortex at an optical bound state in the continuum, *Nat. Photonics* **12**, 397 (2018).
- [8] J. Jin, X. Yin, L. Ni, M. Soljačić, B. Zhen, and C. Peng, Topologically enabled ultrahigh-Q guided resonances robust to out-of-plane scattering, *Nature* **574**, 501 (2019).
- [9] W. Chen, Y. Chen, and W. Liu, Singularities and Poincaré indices of electromagnetic multipoles, *Phys. Rev. Lett.* **122**, 153907 (2019).
- [10] K. Koshelev, A. Bogdanov, and Y. Kivshar, Meta-optics and bound states in the continuum, *Sci. Bull.* **64**, 836 (2019).
- [11] C. Huang, C. Zhang, S. Xiao, Y. Wang, Y. Fan, Y. Liu, N. Zhang, G. Qu, H. Ji, J. Han, Li Ge, Yuri Kivshar, and Qinghai Song, Ultrafast control of vortex microlasers, *Science* **367**, 1018 (2020).
- [12] M. Kang, S. Zhang, M. Xiao, and H. Xu, Merging bound states in the continuum at off-high symmetry points, *Phys. Rev. Lett.* **126**, 117402 (2021).
- [13] M. Kang, L. Mao, S. Zhang, M. Xiao, H. Xu, and C. T. Chan, Merging bound states in the continuum by harnessing higher-order topological charges, *Light Sci. Appl.* **11**, 1 (2022).
- [14] Z. Chen, X. Yin, J. Jin, Z. Zheng, Z. Zhang, F. Wang, L. He, B. Zhen, and C. Peng, Observation of miniaturized bound states in the continuum with ultra-high quality factors, *Sci. Bull.* **67**, 359 (2022).
- [15] M. Kang, Z. Zhang, T. Wu, X. Zhang, Q. Xu, A. Krasnok, J. Han, and A. Alù, Coherent full polarization control based on bound states in the continuum, *Nat. Commun.* **13**, 4536 (2022).
- [16] H. Qin, Y. Shi, Z. Su, G. Wei, Z. Wang, X. Cheng, A. Q. Liu, P. Genevet, and Q. Song, Exploiting extraordinary topological optical forces at bound states in the continuum, *Sci. Adv.* **8**, eade7556 (2022).
- [17] J. Wang, L. Shi, and J. Zi, Spin Hall effect of light via momentum-space topological vortices around bound states in the continuum, *Phys. Rev. Lett.* **129**, 236101 (2022).
- [18] L. Huang, L. Xu, D. A. Powell, W. J. Padilla, and A. E. Miroshnichenko, Resonant leaky modes in all-dielectric metasystems: Fundamentals and applications, *Phys. Rep.* **1008**, 1 (2023).
- [19] H. Zhou, C. Peng, Y. Yoon, C. W. Hsu, K. A. Nelson, L. Fu, J. D. Joannopoulos, M. Soljačić, and B. Zhen, Observation of bulk Fermi arc and polarization half charge from paired exceptional points, *Science* **359**, 1009 (2018).
- [20] W. Liu, B. Wang, Y. Zhang, J. Wang, M. Zhao, F. Guan, X. Liu, L. Shi, and J. Zi, Resonant leaky modes in all-dielectric metasystems: Fundamentals and applications, *Phys. Rev. Lett.* **123**, 116104 (2019).
- [21] A. Chen, W. Liu, Y. Zhang, B. Wang, X. Liu, L. Shi, L. Lu, and J. Zi, Observing vortex polarization singularities at optical band degeneracies, *Phys. Rev. B* **99**, 180101(R) (2019).
- [22] X. Yin, J. Jin, M. Soljačić, C. Peng, and B. Zhen, Observation of topologically enabled unidirectional guided resonances, *Nature* **580**, 467 (2020).
- [23] W. Ye, Y. Gao, and J. Liu, Singular points of polarizations in the momentum space of photonic crystal slabs, *Phys. Rev. Lett.* **124**, 153904 (2020).
- [24] T. Yoda and M. Notomi, Generation and annihilation of topologically protected bound states in the continuum and circularly polarized states by symmetry breaking, *Phys. Rev. Lett.* **125**, 053902 (2020).
- [25] W. Liu, W. Liu, L. Shi, and Y. Kivshar, Topological polarization singularities in metaphotonics, *Nanophotonics* **10**, 1469 (2021).
- [26] Y. Zeng, G. Hu, K. Liu, Z. Tang, and C.-W. Qiu, Dynamics of topological polarization singularity in momentum space, *Phys. Rev. Lett.* **127**, 176101 (2021).
- [27] X. Wang, J. Wang, X. Zhao, L. Shi, and J. Zi, Realizing tunable evolution of bound states in the continuum and circularly polarized points by symmetry breaking, *ACS Photonics* **10**, 2316 (2022).
- [28] N. Shitrit, I. Yulevich, E. Maguid, D. Ozeri, D. Veksler, V. Kleiner, and E. Hasman, Spin-optical metamaterial route to spin-controlled photonics, *Science* **340**, 724 (2013).
- [29] J. Wang, H. Li, Y. Ma, M. Zhao, W. Liu, B. Wang, S. Wu, X. Liu, L. Shi, T. Jiang, and Jian Zi, Routing valley exciton emission of a WS₂ monolayer via delocalized Bloch modes of in-plane inversion-symmetry-broken photonic crystal slabs, *Light Sci. Appl.* **9**, 148 (2020).
- [30] J. Wang, M. Zhao, W. Liu, F. Guan, X. Liu, L. Shi, C. T. Chan, and J. Zi, Shifting beams at normal incidence via controlling momentum-space geometric phases, *Nat. Commun.* **12**, 6046 (2021).
- [31] J. Tian, G. Adamo, H. Liu, M. Klein, S. Han, H. Liu, and C. Soci, Optical Rashba effect in a light-emitting perovskite metasurface, *Adv. Mater.* **34**, 2109157 (2022).
- [32] X. Zhang, Y. Liu, J. Han, Y. Kivshar, and Q. Song, Chiral emission from resonant metasurfaces, *Science* **377**, 1215 (2022).
- [33] T. Shi, Z.-L. Deng, G. Geng, X. Zeng, Y. Zeng, G. Hu, A. Overvig, J. Li, C.-W. Qiu, A. Alù, Yuri S. Kivshar, and Xiangping Li, Planar chiral metasurfaces with maximal and tunable chiroptical response driven by bound states in the continuum, *Nat. Commun.* **13**, 4111 (2022).
- [34] W. Chen, Q. Yang, Y. Chen, and W. Liu, Evolution and global charge conservation for polarization singularities emerging from non-Hermitian degeneracies, *Proc. Natl. Acad. Sci. U.S.A.* **118**, e2019578118 (2021).
- [35] M. Berry and M. Dennis, The optical singularities of birefringent dichroic chiral crystals, *Proc. R. Soc. A* **459**, 1261 (2003).
- [36] A. D. Kiselev, R. G. Vovk, R. I. Egorov, and V. G. Chigrinov, Polarization-resolved angular patterns of nematic liquid crystal cells: Topological events driven by incident light polarization, *Phys. Rev. A* **78**, 033815 (2008).

- [37] I. O. Buinyi, V. G. Denisenko, and M. S. Soskin, Topological structure in polarization resolved conoscopic patterns for nematic liquid crystal cells, *Opt. Commun.* **282**, 143 (2009).
- [38] T. A. Fadeyeva, V. G. Shvedov, Y. V. Izdebskaya, A. V. Volyar, E. Brasselet, D. N. Neshev, A. S. Desyatnikov, W. Krolikowski, and Y. S. Kivshar, Spatially engineered polarization states and optical vortices in uniaxial crystals, *Opt. Express* **18**, 10848 (2010).
- [39] S. Fan and J. D. Joannopoulos, Analysis of guided resonances in photonic crystal slabs, *Phys. Rev. B* **65**, 235112 (2002).
- [40] Y. Chen, H. Deng, X. Sha, W. Chen, R. Wang, Y.-H. Chen, D. Wu, J. Chu, Y. S. Kivshar, S. Xiao, and Cheng-Wei Qiu, Observation of intrinsic chiral bound states in the continuum, *Nature* **613**, 474 (2023).
- [41] H. Terças, H. Flayac, D. D. Solnyshkov, and G. Malpuech, Non-Abelian gauge fields in photonic cavities and photonic superfluids, *Phys. Rev. Lett.* **112**, 066402 (2014).
- [42] S. Richter, T. Michalsky, C. Sturm, B. Rosenow, M. Grundmann, and R. Schmidt-Grund, Exceptional points in anisotropic planar microcavities, *Phys. Rev. A* **95**, 023836 (2017).
- [43] S. Richter, H.-G. Zirnstein, J. Zúñiga-Pérez, E. Krüger, C. Deparis, L. Trefflich, C. Sturm, B. Rosenow, M. Grundmann, and R. Schmidt-Grund, Voigt exceptional points in an anisotropic ZnO-based planar microcavity: Square-root topology, polarization vortices, and circularity, *Phys. Rev. Lett.* **123**, 227401 (2019).
- [44] L. Polimeno, A. Fieramosca, G. Lerario, L. De Marco, M. De Giorgi, D. Ballarini, L. Dominici, V. Ardizzone, M. Pugliese, C. Prontera, V. Maiorano, G. Gigli, C. Leblanc, G. Malpuech, D. D. Solnyshkov, and D. Sanvitto, Experimental investigation of a non-Abelian gauge field in 2D perovskite photonic platform, *Optica* **8**, 1442 (2021).
- [45] M. Król, I. Septembre, P. Oliwa, M. Kędziora, K. Łempicka-Mirek, M. Muszyński, R. Mazur, P. Morawiak, W. Piecek, P. Kula, W. Bardyszewski, P. G. Lagoudakis, D. D. Solnyshkov, G. Malpuech, B. Pietka, and J. Szczytko, Annihilation of exceptional points from different Dirac valleys in a 2D photonic system, *Nat. Commun.* **13**, 5340 (2022).
- [46] K. Rechcińska, M. Król, R. Mazur, P. Morawiak, R. Mirek, K. Łempicka, W. Bardyszewski, M. Matuszewski, P. Kula, W. Piecek *et al.*, Engineering spin-orbit synthetic Hamiltonians in liquid-crystal optical cavities, *Science* **366**, 727 (2019).
- [47] J. Ren, Q. Liao, F. Li, Y. Li, O. Bleu, G. Malpuech, J. Yao, H. Fu, and D. Solnyshkov, Nontrivial band geometry in an optically active system, *Nat. Commun.* **12**, 689 (2021).
- [48] M. Król, K. Rechcińska, H. Sigurdsson, P. Oliwa, R. Mazur, P. Morawiak, W. Piecek, P. Kula, P. G. Lagoudakis, M. Matuszewski, Barbara Pietka, and Jacek Szczytko, Realizing optical persistent spin helix and Stern-Gerlach deflection in an anisotropic liquid crystal microcavity, *Phys. Rev. Lett.* **127**, 190401 (2021).
- [49] P. Kokhanchik, H. Sigurdsson, B. Pietka, J. Szczytko, and P. G. Lagoudakis, Photonic Berry curvature in double liquid crystal microcavities with broken inversion symmetry, *Phys. Rev. B* **103**, L081406 (2021).
- [50] L. Polimeno, G. Lerario, M. De Giorgi, L. De Marco, L. Dominici, F. Todisco, A. Coriolano, V. Ardizzone, M. Pugliese, C. T. Prontera *et al.*, Tuning of the Berry curvature in 2D perovskite polaritons, *Nat. Nanotechnol.* **16**, 1349 (2021).
- [51] Y. Li, X. Ma, X. Zhai, M. Gao, H. Dai, S. Schumacher, and T. Gao, Manipulating polariton condensates by Rashba-Dresselhaus coupling at room temperature, *Nat. Commun.* **13**, 3785 (2022).
- [52] T. Long, X. Ma, J. Ren, F. Li, Q. Liao, S. Schumacher, G. Malpuech, D. Solnyshkov, and H. Fu, Helical polariton lasing from topological valleys in an organic crystalline microcavity, *Adv. Sci.* **9**, 2203588 (2022).
- [53] K. Łempicka-Mirek, M. Król, H. Sigurdsson, A. Winukiewicz, P. Morawiak, R. Mazur, M. Muszyński, W. Piecek, P. Kula, T. Stefaniuk, Maria Kamińska, Luisa De Marco, Pavlos G. Lagoudakis, Dario Ballarini, Daniele Sanvitto, Jacek Szczytko, and Barbara Pietka, Electrically tunable Berry curvature and strong light-matter coupling in liquid crystal microcavities with 2D perovskite, *Sci. Adv.* **8**, eabq7533 (2022).
- [54] J. Jia, X. Cao, X. Ma, J. De, J. Yao, S. Schumacher, Q. Liao, and H. Fu, Circularly polarized electroluminescence from a single-crystal organic microcavity light-emitting diode based on photonic spin-orbit interactions, *Nat. Commun.* **14**, 31 (2023).
- [55] Q. Liang, X. Ma, T. Long, J. Yao, Q. Liao, and H. Fu, Circularly polarized lasing from a microcavity filled with achiral single-crystalline microribbons, *Angew. Chem. Int. Ed.* **135**, e202213229 (2023).
- [56] M. J. Stephen and J. P. Straley, Physics of liquid crystals, *Rev. Mod. Phys.* **46**, 617 (1974).
- [57] R. Dąbrowski, P. Kula, and J. Herman, High birefringence liquid crystals, *Crystals* **3**, 443 (2013).
- [58] K. Lekenta, M. Król, R. Mirek, K. Łempicka, D. Stephan, R. Mazur, P. Morawiak, P. Kula, W. Piecek, P. G. Lagoudakis, Barbara Pietka, and Jacek Szczytko, Tunable optical spin Hall effect in a liquid crystal microcavity, *Light Sci. Appl.* **7**, 74 (2018).
- [59] A. J. Seed, K. J. Toyne, J. W. Goodby, and M. Hird, Synthesis, transition temperatures, and optical properties of various 2,6-disubstituted naphthalenes and related 1-benzothiophenes with butylsulfanyl and cyano or isothiocyanato terminal groups, *J. Mater. Chem.* **10**, 2069 (2000).
- [60] See Supplemental Material at <http://link.aps.org/supplemental/10.1103/PhysRevApplied.20.054059> for methods, design of DBRs, details of Bereeman's transfer-matrix method, detailed evolutions of the polarization distribution, detailed evolutions of reflectance spectra, and further discussions. References [19,43,45,63,64] are also cited in Supplemental Material.
- [61] O. Bleu, D. D. Solnyshkov, and G. Malpuech, Measuring the quantum geometric tensor in two-dimensional photonic and exciton-polariton systems, *Phys. Rev. B* **97**, 195422 (2018).
- [62] A. Gianfrate, O. Bleu, L. Dominici, V. Ardizzone, M. De Giorgi, D. Ballarini, G. Lerario, K. West, L. Pfeiffer, D. Solnyshkov, D. Sanvitto, and G. Malpuech, Measurement of the quantum geometric tensor and of the anomalous Hall drift, *Nature* **578**, 381 (2020).

- [63] D. W. Berreman, Optics in stratified and anisotropic media: 4×4 -matrix formulation, *J. Opt. Soc. Am.* **62**, 502 (1972).
- [64] P. Yeh, A. Yariv, and C.-S. Hong, Electromagnetic propagation in periodic stratified media. I. General theory, *J. Opt. Soc. Am.* **67**, 423 (1977).